Met. Mater. Int., Vol. 21, No. 3 (2015), pp. 531~537
doi: 10.1007/s12540-015-4369-y

Microstructures, Mechanical Properties, and Fracture Behaviors of Metal-Injection Molded 17-4PH Stainless Steel

Ming-Wei Wu[1,*], Zeng-Kai Huang[2], Chun-Feng Tseng[2], and Kuen-Shyang Hwang[3]

[1]Department of Materials and Mineral Resources Engineering, National Taipei University of Technology, No. 1, Sec.3, Zhong-Xiao E. Rd., Taipei 10608, Taiwan, ROC
[2]Department of Materials Science and Engineering, National Formosa University, No. 64, Wunhua Rd., Huwei, Yunlin 63201, Taiwan, ROC
[3]Department of Materials Science and Engineering, National Taiwan University, No. 1, Sec. 4, Roosevelt Rd., Taipei 10617, Taiwan, ROC

(received date: 6 August 2014 / accepted date: 12 December 2014)

Metal injection molding (MIM) is a versatile technique for economically manufacturing various metal parts with complicated shapes and excellent properties. The objective of this study was to clarify the effects of powder type (water-atomized and gas-atomized powders) and various heat treatments (sintering, solutioning, H900, and H1100) on the microstructures, mechanical properties, and fracture behaviors of MIM 17-4PH stainless steels. The results showed that better mechanical properties of MIM 17-4PH can be achieved with gas-atomized powder than with water-atomized powder due mainly to the lower silicon and oxygen contents and fewer SiO_2 inclusions in the steels. The presence of 10 vol% δ ferrite does not impair the UTS or elongation of MIM 17-4PH stainless steels. The δ ferrite did not fracture, even though the neighboring martensitic matrix was severely cracked. Moreover, H900 treatment produces the highest hardness and UTS, along with moderate elongation. H1100 treatment produces the best elongation, along with moderate hardness and UTS.

Keywords: alloys, sintering, microstructure, mechanical properties, tensile test

1. INTRODUCTION

Metal injection molding (MIM) is widely used to fabricate metal parts in the mechanical, computer, communications, consumer electronics, and other fields. MIM combines the advantages of powder metallurgy (PM) and plastic injection molding (PIM) to economically produce various parts with complicated shapes and outstanding performances. The properties of MIM parts are superior to those of PM parts due mainly to the finer original powder used, which results in both a higher sintered density and a more uniform microstructure. Near fully-dense metal parts can be obtained by selecting an adequate raw powder and appropriate processing and sintering parameters. Among the material systems of MIM stainless steels, 17-4PH [1-14], austenite type [15,16], ferrite type [17,18], and duplex type [17,18] stainless steels have been extensively studied, particularly 17-4PH. MIM 17-4PH stainless steel is a promising material for industry because of its superior mechanical and corrosion performances.

Several studies have investigated the effects of powder and feedstock characteristics [1-5], sintering temperature [1,6-10], sintering atmosphere [5,8,10], and additions of alloying elements [11-13] on the densification and properties of MIM 17-4PH. Wu *et al*. [8] investigated the roles of sintering atmospheres (H_2 and H_2+N_2) on the densification of 17-4PH and showed that H_2+N_2 atmosphere retards densification. Chang *et al*. [11] added 0.2~0.3 wt% graphite powder to reduce the amount of silica inclusion in 17-4PH and thereby improved the mechanical properties. Gülsoy *et al*. [12,13] used 1 wt% NiB addition to induce liquid phase sintering and increase the mechanical properties of 17-4PH.

δ ferrite is an important constituent in both wrought and sintered 17-4PH stainless steels. The roles of δ ferrite in the various mechanical properties of wrought martensitic steels with high chromium content have been investigated in several studies [7,19-21]. Schäfer [19] found that δ ferrite in a martensitic steel with 9~14 wt% Cr can increase the ductility and toughness, though the strength is impaired. In contrast, the presence of δ ferrite in wrought 17-4PH leads to lower tensile elongation [7]. Furthermore, Wang *et al*. [20] indicated that increasing δ ferrite content from 0 to 7.8 vol% in a 13Cr-4Ni (wt%) martensitic stainless steel deteriorates the impact performance and increases the ductile to brittle transition

*Corresponding author: mwwu@ntut.edu.tw

temperature (DBTT). However, the impact energy of 12Cr-2Ni (wt%) martensitic steel can be improved by increasing the volume fraction of δ ferrite from 5.5% to 33% [21].

The presence of δ ferrite also affects the sintering behavior [1,7-9] and the mechanical properties [7,14] of sintered 17-4PH stainless steel. The amount of δ ferrite increases when the sintering temperature is increased [1,7-9]. δ ferrite can facilitate the densification and thus the sintered density of 17-4PH due to its BCC structure and high diffusion rate, as demonstrated by Wu *et al*. [8,9]. Suri *et al*. [14] found that the effect of δ ferrite content and its morphology on the impact energy of MIM 17-4PH could be disregarded. On the other hand, Sago *et al*. [7] indicated that reducing δ ferrite increases both the tensile strength and elongation of MIM 17-4PH. The above findings clearly show the importance and complexity of δ ferrite in not only the sintering behavior but also the mechanical properties of MIM 17-4PH. Wu *et al*. [8,9] have identified that δ ferrite facilitates the densification of 17-4PH. However, the role of δ ferrite in the mechanical properties and fracture behaviors of MIM 17-4PH is still unclear.

The type of stainless steel powder used also plays an important role in the sintered density and mechanical properties [1,15]. Suri *et al*. [15] investigated the effects of 316L powder types on sintering and showed that sintering water-atomized and gas-atomized powders at 1360 °C for 1 h in H_2 can achieve 97% and 99% of the theoretical density, respectively. Gülsoy *et al*. [1] indicated that after sintering at 1350 °C for 1 h in H_2, water-atomized and gas-atomized 17-4PH powders can achieve 97.1% and 98.7% of the theoretical density, respectively. However, the influences of powder type on the mechanical properties and fracture behaviors have rarely been examined. In addition, the effects of various heat treatments on the performances of MIM 17-4PH have yet to be clarified. The objective of this study was thus to clarify the influences of powder type (water-atomized and gas-atomized powders) and various heat treatments (sintering, solutioning, H900, and H1100) on the microstructures, mechanical properties, and fracture behaviors of MIM 17-4PH stainless steel. The role of δ ferrite in the mechanical properties is also discussed.

2. EXPERIMENTAL PROCEDURES

The water atomized (Epson Atmix Co.) and gas atomized (Sandvik Osprey Co.) powders used in this study were designated as W and G, respectively. The appearances of these two powders are shown in Fig. 1. The particles of G powder are spherical and slightly more regular than those of W powder.

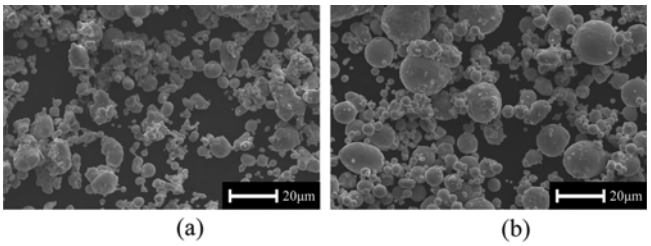

Fig. 1. The appearances of (a) water-atomized and (b) gas-atomized 17-4PH powders.

The chemical compositions and median particle sizes of the two powders are listed in Table 1. The D_{10}, D_{50}, and D_{90} particle sizes of W powders were 4.5, 10.3, and 28.9 μm, respectively. The D_{10}, D_{50}, and D_{90} particle sizes of G powders were 4.3, 12.0, and 28.4 μm, respectively. The differences on the powder size and size distribution between W and G powders were minor and the particle sizes of two original powders should not play a role on the densification. To prepare MIM feedstocks, metal powders were kneaded with 7 wt% wax-based binder consisting of paraffin wax (PW), stearic acid (SA), and polyethylene (PE), using a Σ-blade kneading machine. The resulting feedstock was injection molded into tensile bars as per MPIF Standard 50 using a molding machine (320C/400, Arburg GmbH, Lossburg, Germany).

To remove the organic binder in the green compact, solvent and thermal debinding were used. The compacts were first immersed in heptane at 45 °C for 8 h. Then they were heated at 2 °C/min to 500 °C and held at that temperature for 2 h in a tube furnace under hydrogen. After debinding, the specimens were heated at 10 °C/min to 1000 °C and soaked for 15 min for pre-sintering. Afterwards, the resulting specimens were heated at 5 °C/min to a sintering temperature of 1350 °C and soaked for 2 h in a vacuum furnace under a partial pressure of argon of about 500 Pa. To clarify the effects of various heat treatments on the properties, as-sintered specimens were solution-treated at 1050 °C for 30 min in vacuum, followed by nitrogen quenching at a pressure of 6 bar. The solution-treated specimens were subsequently aged in H900 (482 °C for 1 h) or H1100 (593 °C for 4 h) precipitation hardening conditions, also under vacuum, followed by nitrogen quenching.

The densities of as-sintered specimens were measured using the Archimedes' method. The carbon and nitrogen/oxygen contents of as-sintered specimens were determined using a carbon/sulfur analyzer (EMIA-220V, Horiba, Kyoto, Japan) and an oxygen/nitrogen analyzer (TC-136, LECO, St. Joseph, Michigan, USA), respectively. The sintered densities and car-

Table 1. The chemical compositions and median powder sizes of water-atomized and gas-atomized 17-4PH stainless steel powders

Powder	Cr (wt%)	Ni (wt%)	Cu (wt%)	Mn (wt%)	Si (wt%)	Nb+Ti (wt%)	Mo (wt%)	O (wt%)	N (wt%)	C (wt%)	Median Size (μm)
W	15.7	4.3	3.3	0.82	0.79	0.30	0.03	0.33	<0.01	0.050	10.3
G	16.6	4.6	4.1	0.54	0.44	0.23	0.11	0.075	0.064	0.030	12.0

Table 2. The carbon, oxygen, and nitrogen contents and sintered densities of the two 17-4PH stainless steels after sintering

Powder	Sintered Density (g/cm^3)	C (wt%)	N (wt%)	O (wt%)
W	7.58 ± 0.02	0.01725	0.00108	0.09824
G	7.66 ± 0.03	0.02510	0.00120	0.00391

bon/nitrogen/oxygen contents are shown in Table 2. The carbon/nitrogen contents of 17-4PH produced by W powder were comparable to those produced by G powder. However, the specimens made with W powder obviously had a higher oxygen content after sintering due to the high original oxygen content of the powder.

The apparent hardness was tested using a Rockwell hardness tester (ARK-600, Mitutoyo Co., Tokyo, Japan) in an HRC scale. Tensile tests were performed to measure tensile strength and elongation using a material testing machine (HT-2402, Hung Ta Instrument Co., Taiwan, ROC). The metallographic specimens were ground, polished, and etched with a mixed solution of 40 ml of HCl, 100ml of ethanol, and 5 g of $CuCl_2$. The metallographic specimens and fracture surface of the tensile bars were examined under a scanning electron microscope (SEM, JSM-6360, JEOL, Tokyo, Japan). The volume fractions of δ ferrite in each specimen were calculated using quantitative metallography techniques. In addition, Thermo-Calc software (Thermo-Calc Software, Stockholm, Sweden) coupled with a TCFE3 database was used to calculate the volume fractions of δ ferrite as a function of temperature. To identify the influence of δ ferrite on the mechanical properties and fracture behavior, the tensile fracture path was also analyzed under an optical microscope [22,23]. In addition, an electron probe micro-analyzer (EPMA, JXA-8200SX, JEOL, Tokyo, Japan) was used to clarify the elemental distributions of chromium, nickel, copper, silicon, and oxygen in the MIM 17-4PH stainless steel.

3. RESULTS AND DISCUSSION

3.1. Microstructure

The as-sintered and heat-treated microstructures of MIM 17-4PH produced with the W and G powders are shown in Figs. 2 and 3, respectively. The results show that the microstructure consisted of martensite and δ ferrite, irrespective of powder type and heat treatment. Martensite and δ ferrite were marked by the white arrows in Fig. 2 and 3. δ ferrite with a block shape was dispersed in the martensitic matrix. The precipitates of copper cannot be observed in Figs. 2 and 3 due to their small size. Moreover, a few black particles smaller than 10 μm were clearly found in the W specimens. To identify these black particles and the distributions of alloy elements, EPMA was used to analyze the elemental distributions, as shown in Fig. 4. The results indicated that both silicon and oxygen atoms obviously concentrated on the black particles, indicating these black particles were SiO_2. SiO_2 inclusions have also been found in MIM 17-4PH and 316L stainless steels [11,15]. The W specimens had more SiO_2 inclusions than the G specimens because of their higher silicon and oxygen contents, as shown in Table 1 and 2. Moreover, chromium was rich in δ ferrite because chromium is a ferrite former. In contrast, nickel and copper segregated at the martensite because nickel and copper are austenite formers. During sintering, nickel and copper atoms were mainly distributed in austenite, which subsequently transformed to martensite during cooling from the sintering temperature.

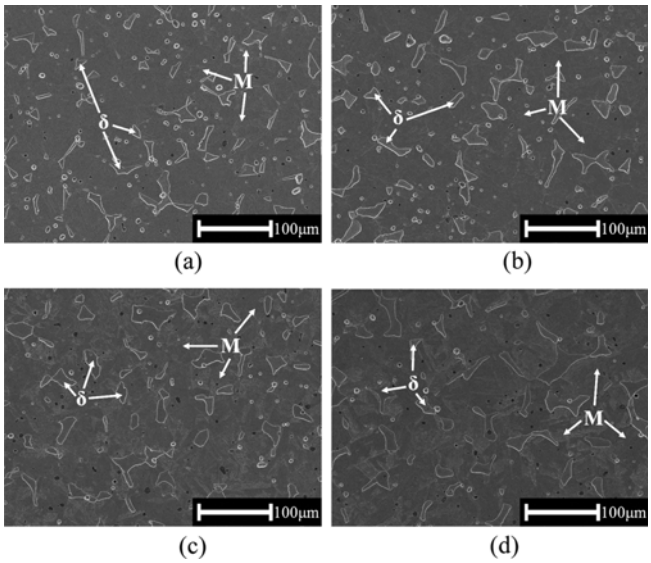

Fig. 2. The microstructures of MIM 17-4PH produced by water-atomized powder (a) as-sintered, (b) solution-treated, (c) H900, and (d) H1100.

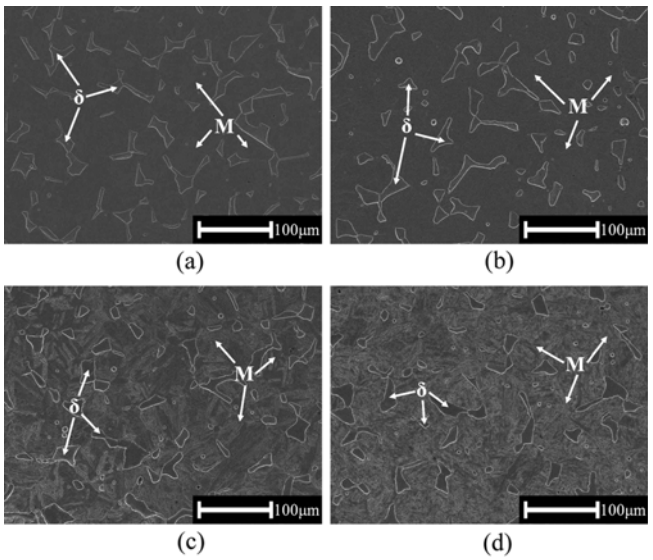

Fig. 3. The microstructures of MIM 17-4PH produced by gas-atomized powder (a) as-sintered, (b) solution-treated, (c) H900, and (d) H1100.

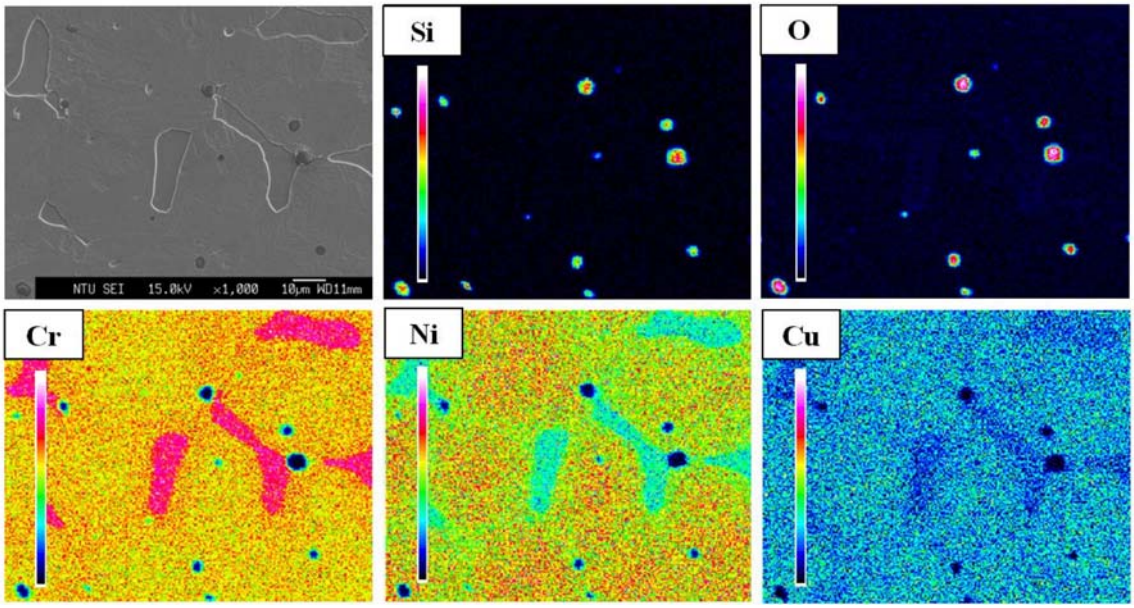

Fig. 4. The elemental mappings of chromium, nickel, copper, silicon, and oxygen in W specimen after H900 treatment.

3.2. Densification

As shown in Table 2, the sintered densities of W and G specimens were 7.58 and 7.66 g/cm^3, respectively. The sintered densities of W specimens were 0.08 g/cm^3 lower than those of G specimens. To understand the influence of δ ferrite on densification, the volume fractions of δ ferrite in each condition were calculated by quantitative metallography. The volume fractions of δ ferrite in the W specimens that were as-sintered, solution-treated, H900-treated, and H1100-treated were 8, 8, 7, and 9%, respectively. The volume fractions of δ ferrite in the G specimens that were as-sintered, solution-treated, H900-treated, and H1100-treated were 8, 12, 13 and 12%, respectively. Thermo-Calc software was also used to simulate the volume fractions of ferrite and austenite in the two specimens as a function of temperature, as demonstrated in Fig. 5. Figure 5 clearly indicates that the fraction of δ ferrite was about 90 vol% at 1350 °C, irrespective of the powder type. This finding shows that δ ferrite did not affect the final sintered density because the difference in the percentages of δ ferrite in the two specimens was minor.

To assess the effect of SiO_2 inclusion on the sintered density, the volume fraction of SiO_2 inclusion was calculated as 1.2 vol% according to the quantitative analyses on the microstructures of W specimens. The theoretical density of 17-PH stainless steel reported in the literature ranges from 7.75 to 7.85 g/cm^3 [14,24-26]. In this study, the theoretical density of 17-PH was regarded as 7.80 g/cm^3. The theoretical density of SiO_2 is only about 2.3 g/cm^3, which is much lower than that of steel matrix. Thus, the theoretical density of 17-4PH made by water-atomized powder should be 7.73 g/cm^3. The presence of 1.2 vol% SiO_2 decreased the theoretical density of MIM 17-4PH from 7.80 to 7.73 g/cm^3. This could be the reason why

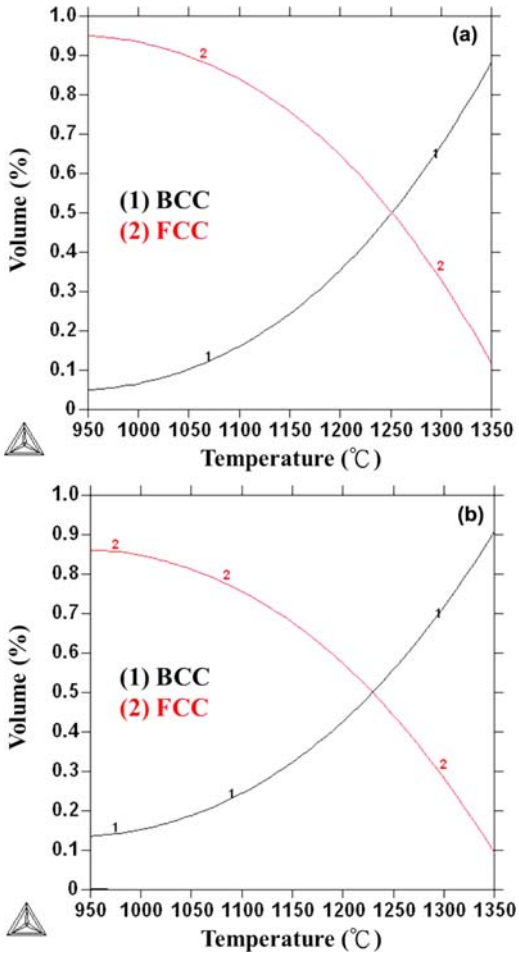

Fig. 5. The simulated volume percentages of ferrite and austenite in (a) W specimen and (b) G specimen as a function of temperature using Thermo-Calc software.

the sintered density of W specimens was 0.08 g/cm^3 lower than that of the G specimens.

3.3. Mechanical properties

The mechanical properties of W and G specimens after various treatments are plotted in Figs. 6-8. Figure 6 indicates that H900 specimens had the highest apparent hardness, followed by H1100, solution-treated, and as-sintered specimens. The type of raw powder did not sufficiently affect the apparent hardness of MIM 17-4PH. The trend of UTS matched that of hardness, as can be seen from comparing Figs. 6 and 7. H900 treatment resulted in the highest UTS, followed by H1100, solution-treated, and as-sintered states. Furthermore, as shown in Fig. 8, H1100 treatment resulted in an elongation greater than 11%, irrespective of the powder type used. The elongations of as-sintered, solution-treated, and H900-treated states were comparable.

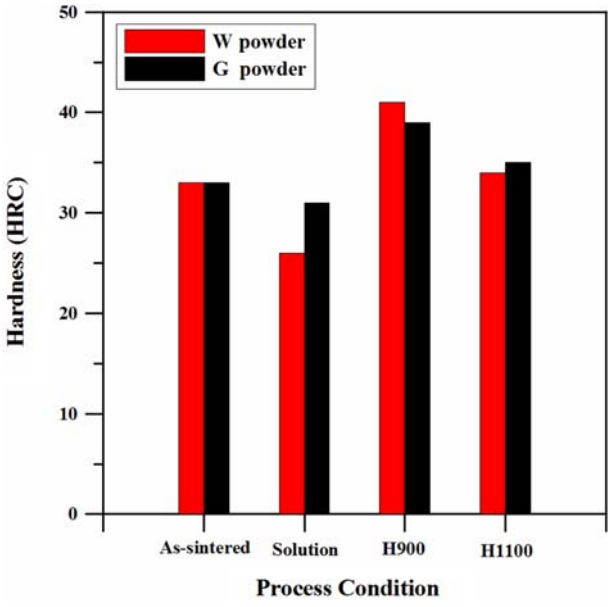

Fig. 6. The apparent hardnesses (HRC) of the two types of MIM 17-4PH as a function of process condition.

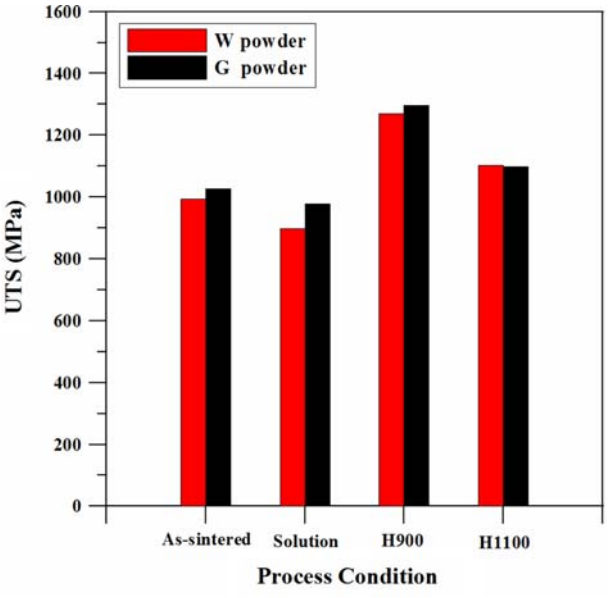

Fig. 7. The ultimate tensile strengths of the two types of MIM 17-4PH as a function of process condition.

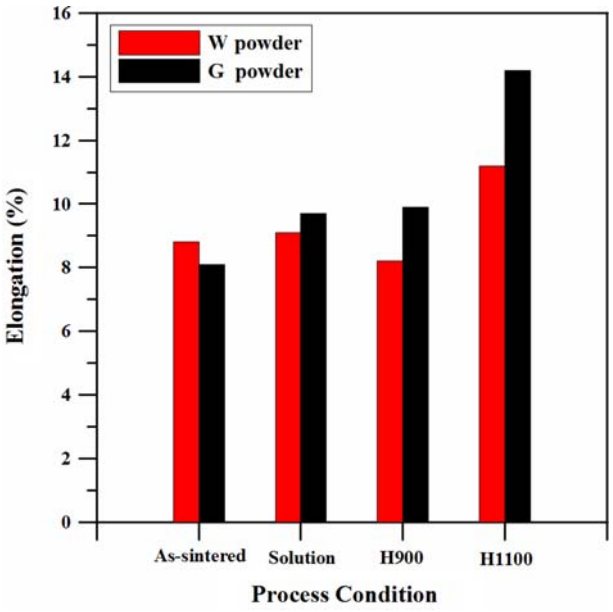

Fig. 8. The tensile elongations of the two types of MIM 17-4PH as a function of process condition.

In general, G specimens exhibited better UTS and elongation than W specimens after a particular treatment. These above findings clearly demonstrate that higher UTS and elongation can be achieved with gas-atomized powder than with water-atomized powder. In addition, H900 treatment resulted in the best combination of UTS and elongation, which was higher than the MPIF specification [27]. The specimens that underwent H1100 treatment had higher elongation and lower hardness and UTS than those that underwent H900 treatment. However, the hardness, UTS, and elongation were better with H1100 treatment than with solution treatment or in the as-sintered state.

3.4. Fracture behavior

Figures 9 and 10 show the tensile fracture surfaces of the W and G specimens after different heat treatments, respectively. The results indicated that ductile fracture occurred in each specimen. However, a large amount of SiO_2 inclusions were found in the dimple of the W specimens. SiO_2 inclusions have also been observed on the fracture surface in several previous studies [1,5-7,11,14]. According to the quantitative analyses, the fracture surfaces of W specimens held 17 SiO_2 inclusions on average per 100 μm×100 μm square. The microstructures of W specimens with various treatments also con-

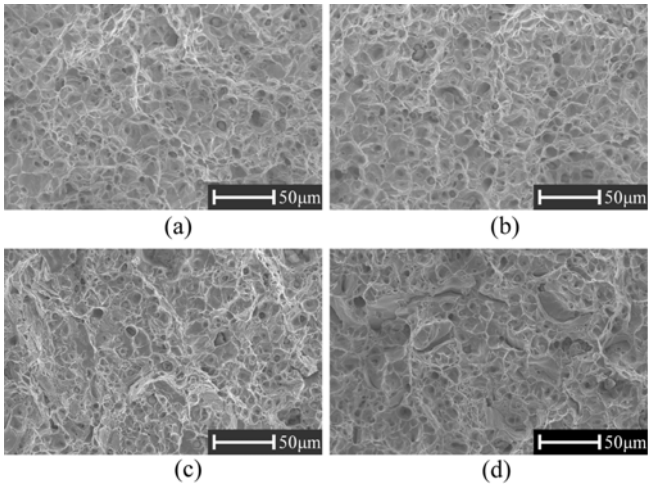

Fig. 9. The tensile fracture surfaces of MIM 17-4PH produced by water-atomized powder (a) as-sintered, (b) solution-treated, (c) H900, and (d) H1100.

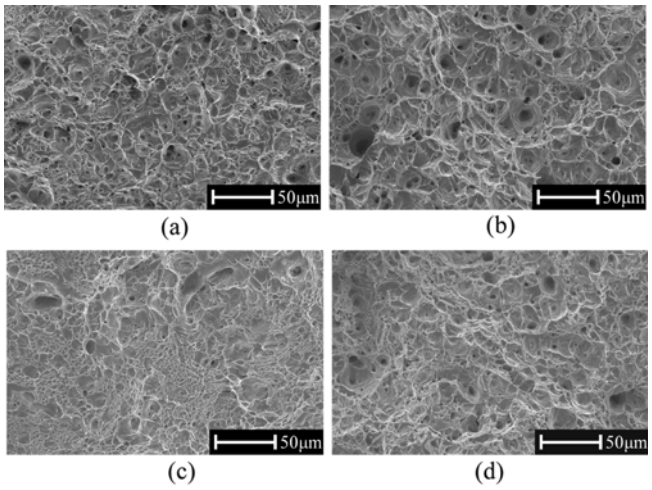

Fig. 10. The tensile fracture surfaces of MIM 17-4PH produced by gas-atomized powder (a) as-sintered, (b) solution-treated, (c) H900, and (d) H1100.

tained many SiO_2 inclusions, as shown in Fig. 2. In contrast, SiO_2 inclusions were rarely found in the G specimens. Unfortunately, the effect of δ ferrite on the fracture could not be clarified from observation of the fracture surface.

To further identify the role of δ ferrite on the mechanical properties and fracture, the tensile fracture path of a W specimen after H900 treatment was examined, as shown in Fig. 11. The fracture path, marked by a white line in Fig. 11(a), occasionally propagated along the δ ferrite but did not tend to follow δ ferrite, indicating that the presence of δ ferrite in the volume fraction of 10% did not deteriorate the mechanical properties of MIM 17-4PH. Moreover, δ ferrite was not fractured, while the neighboring martensitic matrix was severely cracked, as can be seen in the area marked by the square in Fig. 11(b). Thus, it was possible for MIM 17-4PH to achieve

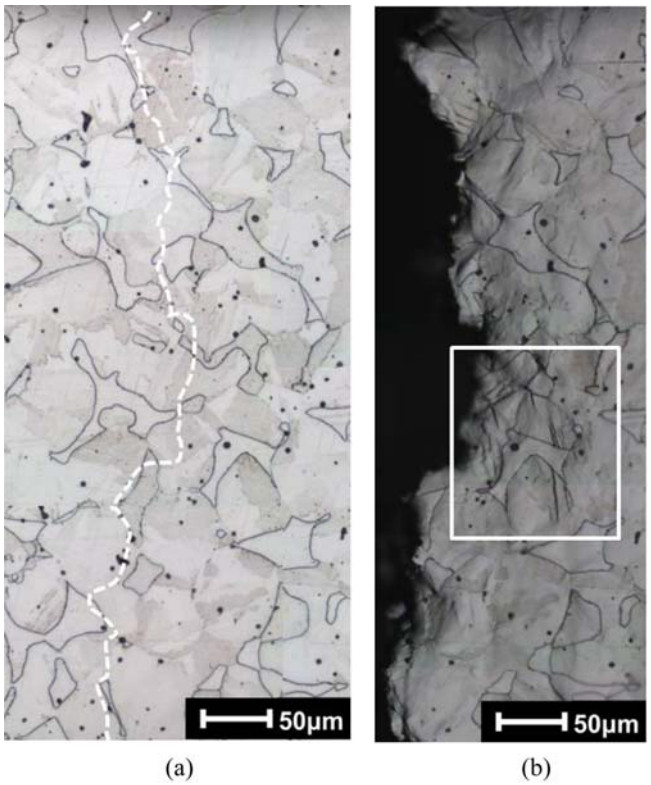

Fig. 11. The tensile fracture path of W specimen after H900 treatment (a) after fracture and (b) before fracture.

excellent mechanical properties in this study.

Gülsoy *et al*. [1] reported that, after H900 treatment, the mechanical properties of 17-4PH made from water-atomized powder were about 10% lower than those made from gas-atomized powder due to the higher porosity. However, in this study, the difference in the porosities between W and G specimens could be neglected, as discussed in section 3.2. According to Chang *et al*. [11], adding 0.26 wt% graphite powder can help reduce SiO_2 inclusion in MIM 17-4PH and then improve the UTS and elongation. During tensile loading, the interface between SiO_2 inclusion and steel matrix will be fractured more easily, and SiO_2 inclusions were thus extensively found on the bottom of dimple in the fracture surface of W specimens, as shown in Fig. 9. Consequently, the lower mechanical properties of W specimens could be mainly attributed to the presence of a large amount of SiO_2 inclusions.

4. CONCLUSIONS

This study identified influences of powder type and various heat treatments on the microstructures, mechanical properties, and fracture behaviors of MIM 17-4PH stainless steel. The findings are summarized as follows.

(1) The mechanical properties of MIM 17-4PH produced by gas-atomized powder are superior to those produced by

water-atomized powder due to the lower silicon and oxygen contents and fewer SiO_2 inclusions.

(2) H900 treatment results in the highest hardness and UTS and moderate elongation of greater than 8%, irrespective of the powder used. H1100 treatment can produce the best elongation, as high as 11%, and moderate hardness and UTS. The mechanical properties of the as-sintered and solution-treated states are lower than those of the H900 and H1100 ones.

(3) The presence of 10 vol% δ ferrite does not impair the UTS or elongation of MIM 17-4PH stainless steels. The δ ferrite did not fracture, even though the neighboring martensitic matrix was severely cracked.

ACKNOWLEDGEMENT

The authors thank the Ministry of Science and Technology of the Republic of China and Taiwan Powder Technologies (TPT) for support under contract number NSC 101-2622-E-150-022-CC3. Our gratitude is also extended to TPT for the preparation of the MIM 17-4PH specimens used in this study.

REFERENCES

1. H. Ö. Gülsoy, S. Özbek, and T. Baykara, *Powder Metall.* **50**, 120 (2007).
2. K. Murray, A. J. Cloeman, T. A. Tingskog, and D. T. Whychell, Sr., *Int. J. Powder Metall.* **47**, 21 (2011).
3. Y. M. Li, L.J. Li, and K. A. Khalil, *J. Mater. Process. Technol.* **183**, 432 (2007).
4. K. A. Khalil and S. W. Kim, *Met. Mater. Inter.* **12**, 101 (2006).
5. S. Banerjee and C. J. Joens, *Adv. Powder Metall. Part. Mater.* **4**, 94 (2008).
6. H. J. Sung, T. K. Ha, S. Ahn, and Y. W. Chang, *J. Mater. Process. Technol.* **130-131**, 321 (2002).
7. J. A. Sago, M. D. Wilson, M. W. Broadley, J. K. Eckert, and R. J. White, *Adv. Powder Metall. Part. Mater.* **4**, 105 (2008).
8. Y. X. Wu, D. Blaine, B. Marx, C. Schlaefer, and R. M. German, *Metall. Mater. Trans. A* **33**, 2185 (2002).
9. Y. X. Wu, R. M. German, D. Blaine, B. Marx, and C. Schlaefer, *J. Mater. Sci.* **37**, 3573 (2002).
10. H. Ye, X. Y. Liu, and H. Hong, *Mater. Lett.* **62**, 3334 (2008).
11. C. W. Chang, P. H. Chen, and K. S. Hwang, *Mater. Trans.* **51**, 2243 (2010).
12. H. Ö. Gülsoy, *Scripta Mater.* **52**, 187 (2005).
13. H. Ö. Gülsoy and S. Salman, *J. Mater. Sci.* **40**, 3415 (2005).
14. P. Suri, B. P. Smarslok, and R. M. German, *Powder Metall.* **49**, 40 (2006).
15. P. Suri, R. P. Koseski, and R. M. German, *Mater. Sci. Eng. A* **402**, 341 (2005).
16. E. Otero, A. Pardo, M. V. Utrilla, E. Sáenz, and J. F. Álvarez, *Corros. Sci.* **40**, 1421 (1998).
17. C. Moral, A. Bautista, and F. Velasco, *Corros. Sci.* **51**, 1651 (2009).
18. C. Garcia, F. Martin, Y. Blanco, and M. L. Aparicio, *Corros. Sci.* **52**, 3725 (2010).
19. L. Schäfer, *J. Nucl. Mater.* **258-263**, 1336 (1998).
20. P. Wang, S. P. Lu, N. M. Xiao, D. Z. Li, and Y. Y. Li, *Mater. Sci. Eng. A* **527**, 3210 (2010).
21. G. Alkan, D. Chae, and S. J. Kim, *Mater. Sci. Eng. A* **585**, 39 (2013).
22. M. W. Wu, G. J. Shu, S. Y. Chang, and B. H. Lin, *Metall. Mater. Trans. A* **45**, 3866 (2014).
23. M .W. Wu, L. C. Tsao, and S. Y. Chang, *Mater. Sci. Eng. A* **565**, 196 (2013).
24. I. Costa, S. O. Rogero, M. Saiki, R. A. Marques, and J. R. Rogero, *Mater. Sci. Forum* **591-593**, 18 (2008).
25. R. Schroeder, G. Hammes, C. Binder, and A. N. Klein, *Mater. Res.* **14**, 564 (2011).
26. M. Dourandish, A. Simchi, E. T. Shabestary, and T. Hartwig, *J. Am. Ceram. Soc.* **91**, 3493 (2008).
27. Metal Powder Industries Federation, *Materials Standards for Metal Injection Molded Parts*, p.19, Metal Powder Industries Federation, New Jersey, USA (2007).